Green emission from barium–strontium titanate matrix introduced into nano-porous anodic alumina

A. Podhorodecki [a],[*], N.V. Gaponenko [b],[1], M. Banski [a], M.V. Rudenko [b],[1], L.S. Khoroshko [b],[1], A. Sieradzki [a], J. Misiewicz [a]

[a] *Institute of Physics, Wroclaw University of Technology, Wybrzeze Wyspianskiego 27, 50-370 Wroclaw, Poland*
[b] *Belarusian State University of Informatics and Radioelectronics, P. Browki Str. 6, 220013 Minsk, Belarus*

A R T I C L E   I N F O

A B S T R A C T

The present paper discusses the optical and electrical properties of $(Ba_{0.6}Sr_{0.3}Ca_{0.1})TiO_3$ (BSCT) doped with Tb^{3+} ions and deposited onto nano-porous anodic alumina using sol–gel method. Photoluminescence (PL), PL time-decay and total photoluminescence excitation spectroscopy data obtained from the structure xerogel/porous anodic alumina are compared with the data obtained for Tb in porous anodic alumina deposited by immersion. It has been shown that the most efficient excitation channel of Tb ions in BSCT xerogel is $4f^8 \rightarrow 5d_14f^7$ transition at 270 nm associated with $5d_1$ low-spin states. In consequence, strong emission band at 545 nm corresponding to $^5D_4 \rightarrow {}^7F_5$ transition characterized by the decay constant of 2 ms has been observed for the samples annealed at above 750 °C. This emission significantly and continuously decreases when the temperature is increased from 10 up to 300 K without any abrupt change. This result correlates with the lack of ferroelectric phase transition and appearance of superparaelectric behavior of BSCT matrix observed with electrical measurements.

© 2012 Elsevier B.V. All rights reserved.

1. Introduction

In recent years barium–strontium titanate (BST) has been intensively investigated for advanced dynamic random access memory (DRAM) and uncooled infrared detector applications [1,2] because of its high dielectric constant and composition-dependent Curie temperature (T_C). Below the T_C, these crystals undergo symmetry lowering distortions. These distortions induced by temperature will transfer cubic BST phase (paraelectric state) to tetragonal phase (ferroelectric state), subsequently to orthorhombic and finally to rhombohedra phase at very low temperatures. In addition, in order to control T_C the BST matrix can be doped with different atoms [3] or it can be reduced to nanometer size where the size effects could be used to control T_C as well.

The BST films are fabricated with the use of pulse laser deposition, chemical vapor deposition and sol–gel technique [4,5] which can be used for the preparation of films as well as nano-powders [6,7]. Unlike dry processes, colloidal solutions deposited by spinning are able to penetrate through the channels of mesoporous matrices, which, after heat treatment, enables the fabrication of a xerogel (dried gel) located within the porous layer of several micrometers in thickness [8,9]. Formation of BST matrix in the channels of the honey-comb structure of porous anodic alumina (PAA) has two main advantages. Firstly, it allows us to reduce the size of the material to nanosized domains. Secondly, if geometry of the substrate is chosen properly, it allows us to use photonics effects to control the emission properties of the film. Matrix confinement in two dimensions reduces the grain sizes distribution and the size of the matrix itself [10]. As a consequence, the crystal phase transitions of the BST matrix can be modified and even superparaelectric phase can be formed [11] when the grains are small enough to form the single domain nanocrystals.

Thus, in this paper, by using a variety of optical and electrical experiments, we examine the application potential of Tb-doped $(Ba_{0.6}Sr_{0.3}Ca_{0.1})TiO_3$ (BSCT) matrix in a porous anodic alumina (PAA) membrane. The matrix has been modified by doping BST with calcium to increase the temperature of the phase transition [12] while doping with Tb makes this material optically active.

2. Experimental

The initial materials were barium acetate [$Ba(CH_3COO)_2$], strontium acetate hemihydrate [$Sr(CH_3COO)_2 \cdot 1/2H_2O$], calcium acetate monohydrate [$Ca(CH_3COO)_2 \cdot H_2O$], terbium acetate hydrate [$Tb(CH_3COO)_3 \cdot 3,3H_2O$] and titanium tetraisoproxide [$Ti(OCH(CH_3)_2)_4$]. Glacial acetic acid (CH_3COOH) and 2-methoxyethanol ($CH_3OCH_2CH_2OH$) were used as solvents. The Ba acetate, Sr acetate,

* Correspondig author. Tel.: +48 713202358.
  E-mail addresses: nik@nano.bsuir.edu.by, artur.p.podhorodecki@pwr.wroc.pl (A. Podhorodecki).
[1] Tel./fax: +375 17 2938869.

Ca acetate and Tb acetate were dissolved in acetic acid and re-fluxed at 110 °C for 0.5 h. After cooling down to room temperature, Ti tetraisoproxide, dissolved in 2-methoxyethanol, was added to the solution. The mixed solution was refluxed and then acetylace-tone ($CH_3COCH_2COCH_3$) and water were added to the solution for stabilization and hydrolysis respectively.

Xerogel films were fabricated by spin-on deposition of the syn-thesized sol on a porous anodic alumina membrane. Porous anodic alumina film was grown on aluminium or silicon wafer. After spin-ning the samples were subjected to drying followed by high tem-perature annealing within the temperature range of 500–900 °C. The samples containing xerogel in PAA are designated as BST:Tb.

In order to recognize the properties of the ions directly intro-duced into BSCT matrix from the ones attached to PAA surface, additional samples with porous anodic alumina films on silicon were fabricated, where terbium was deposited from the solution of terbium nitrates with no sol followed by annealing at 800 °C (see [13] for the details). These samples are designated as PAA:Tb.

The excitation beam light from the xenon lamp (450 W) cou-pled with monochromator (Jobin Yvon TRIAX 180) was focused on the sample. The photoluminescence and PL excitation signals were collected and transmitted by an optical fiber to the spectrom-eter (HR4000 Ocean Optics). The excitation signal obtained has been divided by the light source characteristic. The flash xenon lamp and strobe detector coupled with monochromators (Photon Technology Instruments) were used to observe the time-resolved spectra.

Dielectric measurements were performed by the Novocontrol Alpha impedance analyzer in the frequency range from 0.1 Hz to 1 MHz. Measurements of effective complex dielectric permittivity were performed in the temperature range of 255–360 K at the rate of 1 K/min. P–E hysteresis measurements were done at room temperature using an automatic P–E loop tracer based on Dia-mant–Drenck–Pepinsky circuit.

3. Results and discussion

Typical SEM-images of porous anodic alumina with BSCT xero-gel spinning are presented in Fig. 1. There are three different levels of filling PAA pores with BSCT x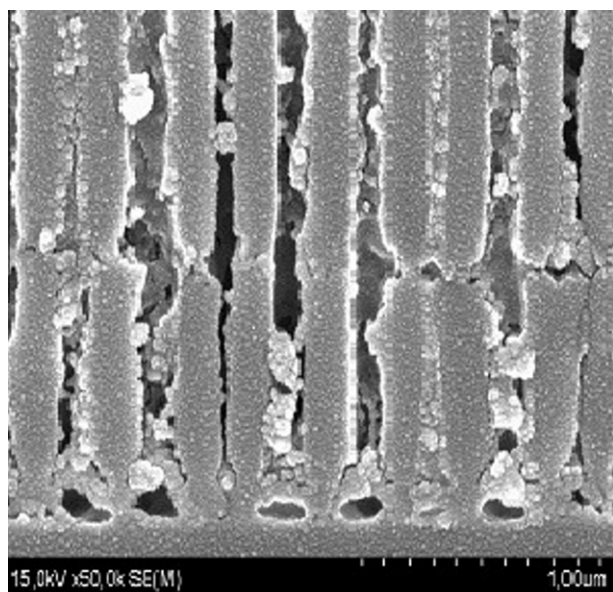erogel. Some of the pores' volume remains almost unfilled with xerogel, some of the pores are filled by the xerogel and most of the pores are partially filled. Neverthe-less, in all cases BSCT xerogel is confined in the volume limited by the pores of ~150 nm in size. It can be also seen on Fig. 1 that the BSCT matrix is formed in porous as grains of approximate sizes of tens of nanometers (~100 nm). This has also been confirmed by XRD patter where additional crystalline phase of perovskite struc-ture ($Ba_{0.6}Sr_{0.4}$)TiO_3 (PDF Card No. 00-034-0411) was detected after annealing the xerogel/porous anodic alumina structure at 750 °C [14].

Fig. 2 shows PL spectra of terbium-doped ($Ba_{0.6}Sr_{0.3}Ca_{0.1}$)TiO_3 (BSCT:Tb) matrices annealed at different temperatures and once obtained from terbium ions directly deposited into the PAA matrix and annealed at 800 °C (PAA:Tb). As it can be seen for BSCT:Tb samples, only samples annealed at high temperatures (750 and 900 °C) reveal well-resolved PL bands at 488, 543, 584 and 621 nm, corresponding to $^5D_4 \rightarrow {}^7F_j$ (j = 6, 5, 4, 3) transitions of Tb^{3+} ions, while for the sample annealed at 600 °C only one broad and defect-related band, centered at 500 nm has been observed [15]. Moreover, when the annealing temperature increases from 750 up to 900 °C, the Tb related emission intensity increases by factor 10. This result correlates with the formation of crystalline phase of perovskite ($Ba_{0.6}Sr_{0.4}$)TiO_3 registered by X-ray diffraction for the undoped BST film annealed at above 750 °C [14]. Below this temperature only amorphous phase has been observed.

Considering the luminescence of lanthanides from the structure xerogel/porous anodic alumina, it should be clarified that like in the case of porous silicon [16], the lanthanide ions can occupy sites not only in xerogel host but at the surface of porous alumina as well [13]. To verify this possibility and to confirm introducing Tb ions into the BSCT matrix, emission spectra for the PAA:Tb sample have also been measured and presented in Fig. 2. Significant emis-sion from Tb ions can be also observed in this case, indicating that important contribution from porous surface sites should be also expected for the BSCT matrix.

In order to understand better the optical properties of the BSCT matrix, the excitation–emission maps have been recorded for BSCT:Tb samples annealed at 750 and 900 °C. Fig. 3a and c shows that apart from the main emission band centered at 545 nm, broad emission band can be observed when both samples are excited above 350 nm. This band is overlapping with the one observed in PL for the sample annealed at 600 °C (see Fig. 3) and has been related to the optically active defect states present in the BSCT
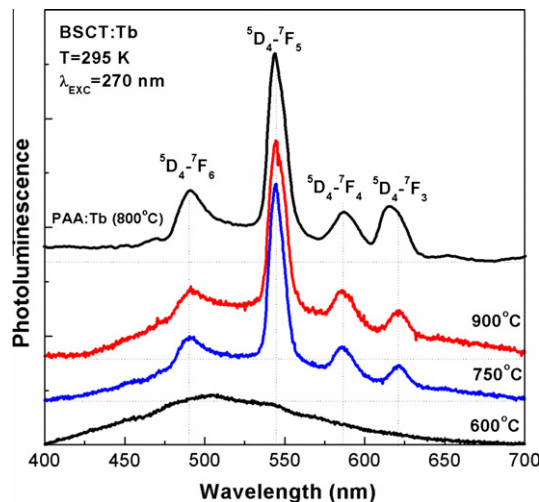

Fig. 1. Typical SEM images of the structure BSCT-xerogel/porous anodic alumina annealed at the temperature of 750 °C.

Fig. 2. Room-temperature PL spectra of Tb-doped barium–strontium–calcium titanate xerogel in porous anodic alumina film fabricated on silicon wafer.
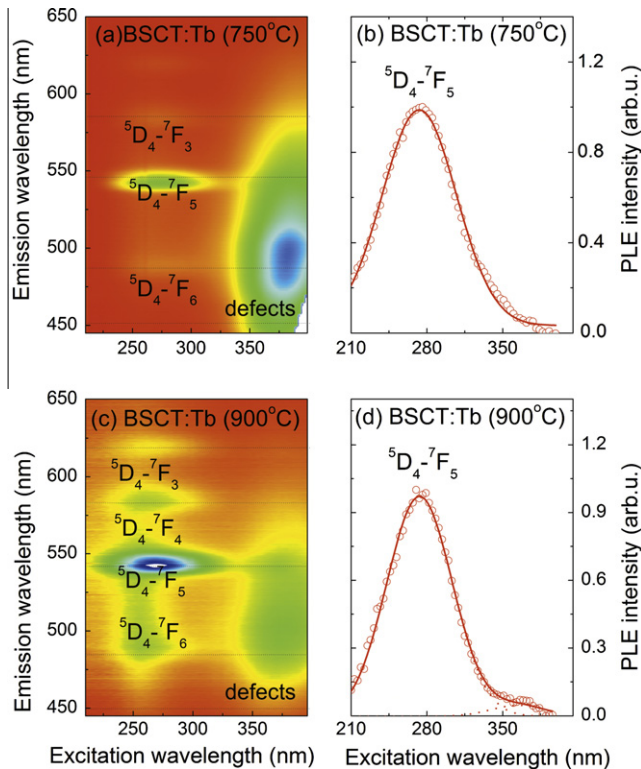
Fig. 3. Excitation–emission maps obtained for BSCT:Tb samples annealed at 750 and 900 °C (a and c). Excitation spectra obtained for $^5D_4$–$^7F_5$ Tb^{+3} emission line for the samples annealed at 750 and 900 °C (b and d).

Fig. 4. (a) TPLE spectra recorded at different temperatures for the PAA:Tb sample annealed at 800 °C and (b) TPLE spectra obtained for the BSCT:Tb sample annealed at 900 °C together with the fitting curves.

matrix. Spectral overlap between this emission band and the emission band related to Tb ions complicate the excitation signal which, recorded at 545 nm ($^5D_4 \rightarrow {}^7F_5$), is now a superposition of the excitation profiles of Tb as well as of the defect states. Thus, to obtain the excitation profile of Tb ions only, the obtained signal has been corrected by the signal recorded for defect related emission only. The excitation spectra obtained this way for Tb ($^5D_4 \rightarrow {}^7F_5$) are shown in Fig. 3b and d. For the BSCT:Tb sample annealed at 900 °C the excitation profile of Tb ions consists of two excitation bands: the main band is centered at 270 nm (4.58 eV) and is characterized by 70 nm (1.17 eV) broadening and the second excitation band is centered at 370 nm (3.34 eV). The excitation spectrum for the BSCT:Tb sample annealed at 750 °C is very similar. In this case however, the main band centered at 276 nm (4.48 eV) is broadened (79 nm (1.36 eV)), which makes it difficult to distinguish the second excitation band at lower energies.

Thus, to investigate the excitation mechanism of Tb^{3+} ions in the BSCT matrix, we focused our attention only on the sample annealed at 900 °C and the PAA:Tb sample. For these samples the excitation spectra have been recorded at different temperatures (10–300 K). Fig. 4 shows the PLE spectra recorded for the BSCT:Tb (900 °C) sample and additionally for the PAA:Tb sample at different temperatures for the main $^5D_4 \rightarrow {}^7F_5$ transition of Tb^{3+} ion.

From Fig. 4 it can be seen that for the PAA:Tb sample two well separated Gaussian-type excitation bands appear at 235 (5.27 eV) and 280 nm (4.41 eV) while for the BSCT sample similar but asymmetric bands appear at 270 nm (4.58 eV) and 370 nm (3.34 eV).

In gaseous form, the first allowed f–d transition for Tb^{3+} is at about 200 nm (6.2 eV) [26]. However, the energy of the first dipole-allowed f–d transition is lowered whenever the lanthanide ion is doped in a host crystal and this value changes from matrix to matrix. Since this value is close to the one obtained for the PAA:Tb sample, the observed excitation bands can be interpreted
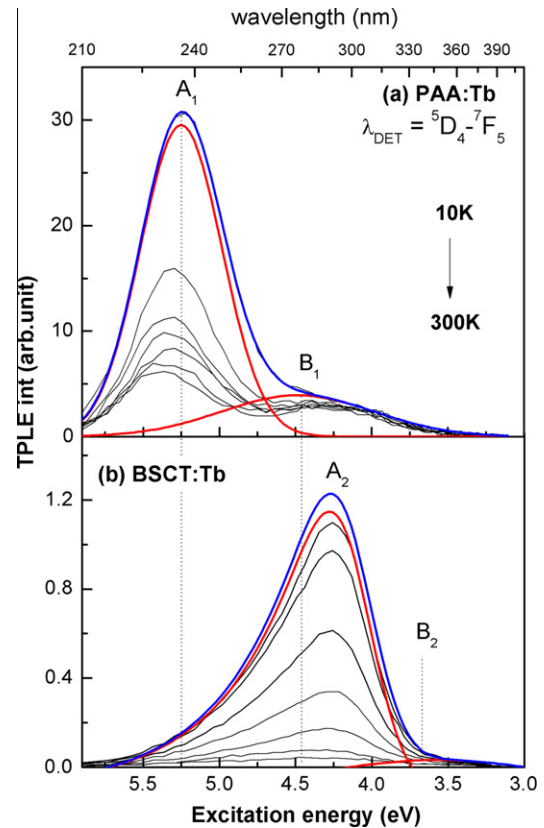
as 4f–5d transitions of Tb^{3+} ions. In more detail, these two bands: 235, 280 nm can be related to 5d$_1$[LS] (low spin) transition and 5d$_1$ [HS] (high spin) transition respectively. Very similar positions of the excitation bands have been already recorded for Tb^{3+} in TbBO$_3$ matrix where the low spin and high spin excitation bands have been observed at 5.28 and 4.44 eV respectively [17]. This suggests that in our case we most probably deal with Tb ions formed at the porous walls in the oxide form.

Following this interpretation, it has been proposed that excitation bands observed for the BSCT:Tb sample are also related to f–d transition of Tb^{3+} ion. In this case however, the main 5d$_1$[LS] transition is strongly redshifted from the position characteristic of a free ion (D = 1.62 eV) and splitting between the low spin and high spin transition (ΔE_{HS-LS}) is higher ~9989 cm^{-1} (1.24 eV) than for the PAA:Tb sample where it amounts to ~6839 cm^{-1} (0.89 eV). Additionally, the ratio between HS and LS transition intensities has been also calculated and is equal to 0.1 (0.1) and 0.2 (0.7) for BSCT:Tb and PAA:Tb samples at 10 K (300 K) respectively. Dorenbos [18,19] collected data on the position of the most intense spin-forbidden transition band for Tb^{3+} in a wide variety of inorganic compounds, and gave an average value of the energy difference between the lowest spin-allowed f–d and the most intense spin-forbidden state bands amounting to 6300 ± 900 cm^{-1}. But the values of ΔE_{HS-LS} are very different for the various compounds; for example ΔE_{HS-LS} = 3400 cm^{-1} for LaPO$_4$ [18] and ΔE_{HS-LS} = 8177 cm^{-1} for YLiF$_4$ [19]. The values obtained for the PAA:Tb sample seems to be in excellent agreement with the averaged value given by Dorenbos. However, $\Delta E_{HS-LS} \approx 10\,000$ cm^{-1} is significantly higher than the values reported so far for other Tb^{3+} hosts. This result could be related to the complexity of the excitation signal but could also constitute a consequence of unique

chemical properties of the BSCT matrix itself or its ferroelectrics properties, where the onset of spontaneous polarization occurs at room temperature and zero field.

To analyze the obtained data in more detail, PLE spectra have been fitted by Gaussian curves defined as follows:

$$G(E) = \frac{A}{\gamma_0} \sqrt{\frac{4\ln 2}{\pi}} \exp\left[-4\ln 2 \left(\frac{E-E_0}{\gamma_0}\right)^2\right]$$

and modified to reflect the asymmetry of excitation band lineshape by replacing γ_0 with a well behaved function, $\gamma(E)$ [20]

$$\gamma(E) = \frac{2\gamma_0}{1 + \exp(a \cdot (E - E_0))}$$

The parameter a is a measure of asymmetry. Negative values of a skew the spectrum towards higher energies while positive values of a skew it towards lower values. When a is zero, it reduces to γ_0 and the resulting band is a standard symmetric Gaussian profile with a constant width (FWHM = γ_0).

The fitting parameters obtained is such a way have been plotted in Fig. 5. As we can see from Fig. 5a, broadening of $5d_1$[LS] excitation band of Tb ions in the BSCT matrix increases by a factor of 2 with the increase of temperature from 10 to 300 K. For the PAA:Tb sample, (see Fig. 5b) broadening of $5d_1$[LS] excitation band is almost constant when the temperature is changing from 10 to 300 K and is equal to ~0.65 eV. Additionally, for the BSCT:Tb sample the position of excitation band related to $5d_1$[LS] is blue-shifted with 140 meV while $5d_1$[HS] band is red-shifted with 410 meV. Similar trends have been obtained for the PAA:Tb sample where blueshift was only 60 meV while redshift was 150 meV.
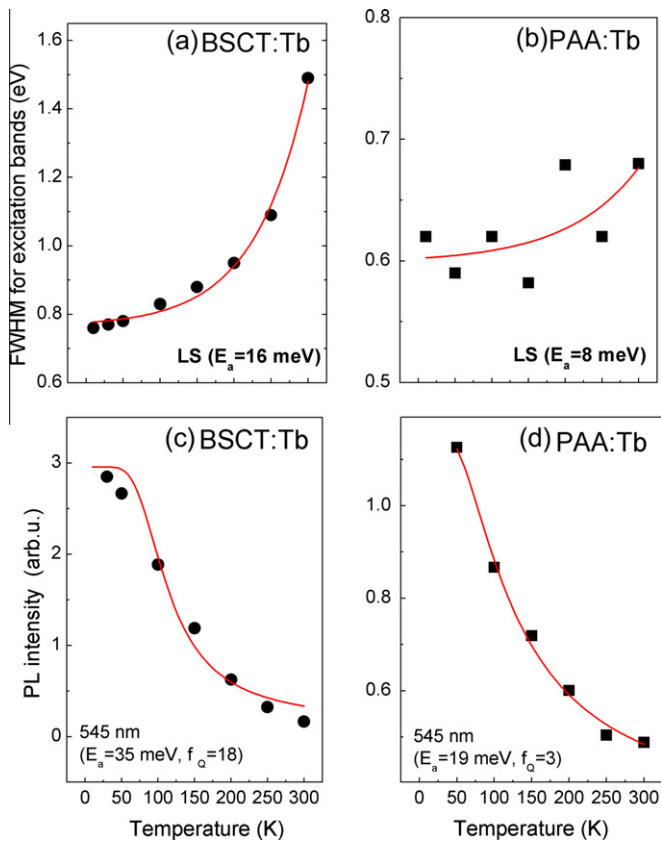
In addition to the excitation spectra recorded at different temperatures, emission intensity for the main $^5D_4 \rightarrow {}^7F_5$ transition at 545 nm for the PAA:Tb and BSCT:Tb (900 °C) samples has been recorded as a function of temperature at excitation to $5d_1$ [LS] level. From Fig. 5c it can be seen that the emission for the BSCT:Tb sample decreases by a factor of 18 with quenching energy of 35 meV. Contrary to this strong quenching observed for the BSCT:Tb sample, intensity of the emission band observed for the PAA:Tb sample decreases only by a factor of 3 with quenching energy of 19 meV. This strong emission quenching observed for the BSCT:Tb sample can be related to the temperature induced changes in local crystal field or efficient coupling of Tb^{3+} ions to defect states present in BSCT matrix. In addition, a significant abrupt change in the emission intensity of Tb^{3+} has been expected (but not observed) due to the expected phase transition in the range of measured temperatures (300–10 K). To explain the lack of this behavior the temperature dependence of the dielectric permittivity and the dielectric loss have been measured for the sample annealed at 900 °C and the results obtained have been shown in Fig. 6.

Fig. 6 shows the temperature dependence of the sample effective dielectric permittivity and the dielectric loss of the BSCT:Tb sample annealed at 900 °C. A decrease of permittivity with the increase of the frequency is observed in the investigated temperature range. Loss values show a continuous decrease with the frequency increase in a whole interval. At lower frequencies values and at greater temperatures the observed increase of the loss could be attributed to the thermally activated conductivity. No anomaly indicating a phase transition in the measured BSCT sample was observed. The lack of phase transition may be attributed to the size effect (due to matrix confinement in the PAA matrix) which reduces and smears a anomalies related to phase changes and finally leads to the disappearance of ferroelectric phase. To confirm this observation, P–E loop has been measured for the sample annealed at 900 °C. The result obtained (see inset in Fig. 6b)
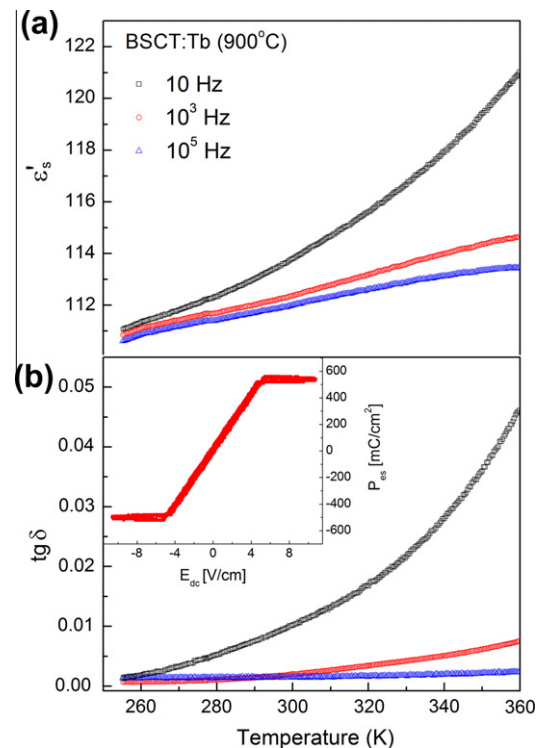

Fig. 5. FWHM of $5d_1$ [LS] excitation band for (a) BSCT:Tb sample annealed at 900 °C and for (b) PAA:Tb sample annealed at 800 °C. PL intensity of $^5D_4-{}^7F_5$ emission band of Tb^{3+} ions recoded as a function of temperature for (c) PAA:Tb and (d) BSCT:Tb samples at excitation to $5d_1$ [LS] state of Tb ions.

Fig. 6. Temperature dependence of the dielectric permittivity and the dielectric loss for the 900° sintered BSCT sample. Inset: P–E loop of the BSCT:Tb.
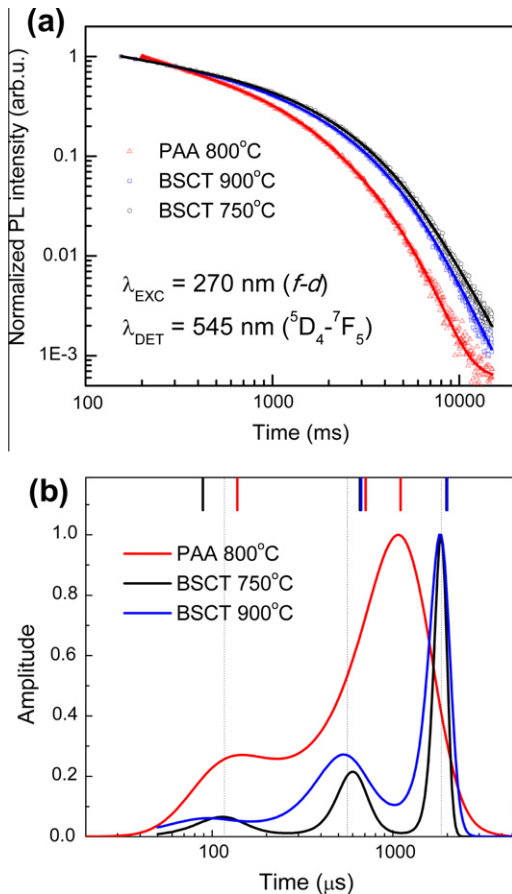
Fig. 7. (a) Emission decay curves and (b) decay times distributions obtained from Maximum Entropy Method for the PAA:BSCT:Tb samples annealed at 750 °C and 900 °C and for the PAA:Tb sample annealed at 800 °C.

unambiguously demonstrates that this BSCT:Tb sample shows unique superparaelectric properties, which is consistent with the theoretical prediction of the ensemble of ferroelectric nanoparticles [21]. The answer about the origin of this superparaelectricity in this sample requires further studies but is probably related to the size effect. Similar effect has been observed by Cheng et al. for $Ba_{0.8}Sr_{0.2}TiO_3$ annealed at 750 °C. For the films with 100–200 nm columnar structure typical hysteresis has been observed, while for the structure with grains of 30–50 nm, the hysteresis saturation observed [22] was similar to that found in our case. Nevertheless, to explore these size effects and their influence on ferroelectric as well as optical properties further studies are necessary, which are already in progress.

In the last step, kinetic properties of Tb^{3+} ions doped into BSCT matrix have been investigated by using time resolved spectroscopy. For this purpose, all BSCT and PAA:Tb samples have been excited at 270 nm ($4f$–$5d_1$[LS]) respectively and the decay curves thus obtained for the most intense $^5D_4$–$^7F_5$ transition have been presented in Fig. 7a. In order to fit the obtained data the Maximum Entropy Method (MEM) has been used [23] and the resulting decay times distribution have been presented in Fig. 7b. From these results we can see that for both BSCT:Tb samples Tb^{3+} emission decay has contribution from three different processes with characteristic decay constants: $\tau_1 \sim 100\ \mu s$, $\tau_2 \sim 600\ \mu s$ and $\tau_3 \sim 1800\ \mu s$. For the PAA:Tb sample however, there are only two

contributions with $\tau_1' \sim 100\ \mu s$ and $\tau_2' \sim 1000\ \mu s$. Based on the obtained result we conclude that the only decay constant related to the recombination of Tb^{3+} ions in the BSCT matrix is $\tau_3 \sim 1800\ \mu s$. The other two decay times we attributed to the recombination of Tb^{3+} ions placed at the PAA porous walls like in the case of the PAA:Tb sample. Additionally, comparing amplitudes of decay times distributions and following our interpretation regarding the origin of decay times, we can conclude that ~80% of Tb ions in the BSCT:Tb sample are introduced into the matrix. The other 20% are the ions which are placed at the porous surface in the oxide-like environment.

4. Conclusion

In conclusion, it has been shown that terbium ions have been successfully introduced into $(Ba_{0.6}Sr_{0.3}Ca_{0.1})TiO_3$ matrix embedded into the PAA matrix. The structures thus obtained are characterized by a strong green emission where the highest intensity is achieved when ions are excited via low spin 5d transition of Tb^{3+} ion at 270 nm. Additionally, it has been shown that this emission depends strongly on the temperature and reduces by factor 18 when the temperature is changing from 10 up to 300 K. Moreover, it has been experimentally shown for the first time that our samples are characterized by superparaelectricity effect induced most probably by the size effect being a consequence of the confinement of the BSCT matrix in the PAA matrix.

References

[1] G.W. Dietz, M. Schumacher, R. Waser, S.K. Streiffer, C. Basceri, A.I. Kingon, J. Appl. Phys. 82 (1997) 2359.
[2] Hyun-Ji Noh, Sung-Gap Lee, Young-Hie Lee, J. Ceram. Process. Res. 9 (2008) 172.
[3] H. Liu, B. Cao, C. O'Connor, J. Appl. Phys. 109 (2011) 07B516.
[4] V.A. Vasiljev, K.A. Vorotilov, M.I. Yanovskaya, L.I. Solovjeva, A.S. Sigov, J. Sol–Gel Sci. Tech. 13 (1998) 877.
[5] A.S. Sigov, K.A. Vorotilov, J. Sol–Gel Sci. Tech. 2 (1994) 256.
[6] G.J. Hu, J. Chen, D.L. An, J.H. Chu, N. Dai, Appl. Phys. Lett. 86 (2005) 162905.
[7] X.K. Hong, G.J. Hu, J.L. Shang, J. Bao, J.H. Chu, N. Dai, Appl. Phys. Lett. 90 (2007) 251911.
[8] R. Herino, Mater. Sci. Eng. B. 69 (2000) 77.
[9] N.V. Gaponenko, Synth. Met. 124 (2001) 125.
[10] N.V. Gaponenko, I.S. Molchan, G.E. Thompson, P. Skeldon, A. Pakes, et al., Sens. Actuators, A 99 (2002) 71.
[11] A. Rudiger, T. Schneller, A. Roelofs, S. Tiedke, T. Schmitz, R. Waser, Appl. Phys. A 80 (2005) 1247.
[12] S.-S. Lim, M.-Soo Han, S.-R. Hahn, S.-G. Lee, Jpn. J. Appl. Phys. 39 (2000) 4835.
[13] N.V. Gaponenko, Y.V. Hluzd, G.K. Malyarevich, I.S. Molchan, G.E. Thompson, et al., Mater. Lett. 63 (2009) 621.
[14] T. Kim, N.V. Gaponenko, E.A. Stepanova, G.K. Maliarevich, A.V. Mudryi, J. Appl. Spect. 76 (2009) 542.
[15] I.A. Souza, M.F.C. Gurgel, L.P.S. Santos, Chem. Phys. 322 (2006) 343.
[16] L. Brewer, in: S.P. Sinha (Ed.), Systematics and the Properties of the Lanthanides, D. Reidel Publishing, Dordrecht, The Netherlands, 1983, p. 17.
[17] R.C. Ropp, B. Carroll, J. Phys. Chem. 81 (1977) 746.
[18] P. Dorenbos, J. Lumin. 91 (2000) 91.
[19] P. Dorenbos, J. Lumin. 91 (2000) 155.
[20] A.L. Stancik, E.B. Brauns, Vib. Spectrosc. 47 (2008) 66.
[21] M.D. Glinchuk, E.A. Eliseev, A.N. Morozovska, Phys. Rev. B 78 (2008) 134107.
[22] J.-G. Cheng, X.-J. Meng, J. Tang, S.-Ling Guo, J.-Hao Chu Min Wang, H. Wang, Z. Wang, J. Am. Ceram. Soc. 83 (2000) 2616.
[23] J.R. Lakowicz, Principles of Fluorescence Spectroscopy, Springer, 2006.